Research article

Downregulated *ATP6V1B1* expression acidifies the intracellular environment of cancer cells leading to resistance to antibody-dependent cellular cytotoxicity

Running title: Intracellular acidification and loss of antitumor immunity

Mariko Nishie[1], Eiji Suzuki[1], Masakazu Hattori[2], Kosuke Kawaguch[1], Tatsuki R. Kataoka[3], Masahiro Hirata[3], Fengling Pu[1], Takeshi Kotake[1], Moe Tsuda[1], Ayane Yamaguchi[1], Tomoharu Sugie[4], Masakazu Toi[1]

[1]Department of Breast Surgery, Graduate School of Medicine, Kyoto University, Kyoto, Japan

[2]Department of Immunosenescence Graduate School of Medicine, Kyoto University, Kyoto, Japan

[3]Department of Diagnostic Pathology, Kyoto University Hospital, Kyoto, Japan

University, Kyoto, Japan

[4]Department of Breast Surgery, Kansai Medical University, Osaka, Japan

Financial support

This research was supported by a grant from the Japan Society for the Promotion of Science (KAKENHI Grant Number 24591901).

Corresponding author: Eiji Suzuki

Department of Breast Surgery, Kyoto University Hospital

54 Shogoin-kawaharacho, Sakyo-ku, Kyoto 606-8507, Japan

Phone +81-75-751-3660

Fax: +81-75-751-3616

Email: eijis@kuhp.kyoto-u.ac.jp

Conflicts of interest:

The authors declare no conflicts of interests in the authorship or publication of this article.

Word count (excluding references): 4163

Figures:7

Table:1

Supplementary Figures:3

Supplementary Table:1

Abstract

Among several mechanisms for the resistance of human epidermal growth factor receptor 2-overexpressing (HER2+) cancer cells to trastuzumab, little is known regarding the mechanism underlying the resistance to trastuzumab-mediated antibody-dependent cellular cytotoxicity (ADCC). Cell death due to ADCC is caused by apoptosis of target cells induced by granzymes released from natural killer cells. Because optimal granzyme physiological activity occurs at neutral pH, we assumed that the pH of the intracellular environment influences the cytotoxic effects of granzymes. We established ADCC-resistant cells and compared them with wild-type cells in terms of the expression of intracellular pH-regulating genes. The expression of *ATP6V1B1*, which encodes a component of vacuolar ATPases, was downregulated in the ADCC-resistant cells. Thus, to functionally characterize ATP6V1B1, we used a CRISPR/Cas9 system to generate *ATP6V1B1*-knockout SKBR3 and JIMT-1 cells (both HER2+ human breast cancer cell line). The resulting cells exhibited significantly less ADCC than the control SKBR3 and JIMT-1 cells. The intracellular pH of the *ATP6V1B1*-knockout SKBR3 and JIMT-1 cells was significantly lower than control SKBR3 and JIMT-1cells. An analysis of granzyme dynamics during the ADCC reaction in cancer cells revealed that granzymes degraded intracellularly in the control SKBR3 and JIMT-1 cells and accumulated in *ATP6V1B1*-knockout cells, but were not cytotoxic. These findings suggest that decreased vacuolar

ATPase activity alters the cytoplasmic pH of cancer cells to create an environment that is less suitable for granzyme bioactivity, which adversely affects the induction of apoptosis of cancer cells by NK cells.

Introduction

Human epidermal growth factor receptor 2-overexpressing (HER2+) breast cancer accounts for 15%–25% of all breast cancer cases and is associated with poor prognosis because of its high proliferation and metastatic potency. However, treatment with trastuzumab, which is a humanized anti-HER2 monoclonal antibody with antitumor activity, have markedly improved the prognosis for patients with HER2+ breast cancer. On the other hand, most patients with metastatic disease who initially respond to trastuzumab generally acquire resistance within 1 year[1], and 20% of patients who receive adjuvant trastuzumab therapy relapse[2].

Trastuzumab blocks intracellular signaling caused by the dimerization of HER2 (including HER2 homologs) with HER family members, including HER3[3]. Thus, trastuzumab-resistance mechanisms are thought to be related to a lack of the extracellular domain of p95HER2[4,5], blockage of the trastuzumab-binding site by membrane-bound mucin (MUC4)[6], alternative signaling from the insulin-like growth factor receptor[7], and activation of the PI3K/AKT pathway via PTEN deletion[8]. Additionally, antitumor immune system processes, especially antibody-dependent cellular cytotoxicity (ADCC), are reportedly crucial[9] for the mechanisms underlying trastuzumab activity. The mechanism of immune-mediated resistance associated with ADCC has been reported to be

correlated with the selective escape of cancer stem cell phenotype[10], the degradation of HER2[11], and FC γ R gene polymorphisms[12,13], however it remains unclear.

The initiation of the ADCC reaction results in the extracellular release of perforin and granzymes from activated natural killer (NK) cells and the subsequent internalization by target cells via endocytosis[10]. Granzymes are inactive in the acidic environment of vacuoles, but are active in a neutral environment (pH 7.5), such as that found in the cytoplasm of target cells[11]. Moreover, V-ATPase, which is located in the plasma membrane and the membrane of organelles (e.g., endosomes, vesicles, and lysosomes), is an important proton transporter that regulates cytosolic and intravesicular pH[12]. We revealed the downregulated expression of the gene encoding V-ATPase by comparing the gene expression of parental breast cancer cells and trastuzumab-mediated ADCC-resistant cells that we established. We hypothesized that decreased V-ATPase functions cause the cytoplasmic pH of cancer cells to change so the cellular environment is no longer suitable for granzyme bioactivity, thereby preventing the induction of apoptosis and impairing the cell-killing action of NK cells. Therefore, in this study, we investigated the mechanism underlying trastuzumab-mediated resistance in cancer cells by focusing on the role of V-ATPase expressed in cancer cells.

Materials and methods

Cell lines

The SKBR3, BT474, JIMT-1(HER2+ human breast cancer cell line) cells, MDA-MB-231 (EGFR-overexpressing triple-negative human breast cancer cell line) cells, and the NCI-N87 (HER2+ human gastric cancer cell line) cells were obtained from the American Type Culture Collection (Manassas, VA). The SKBR3 and NCI-N87 cells were maintained in RPMI 1640 cell culture medium, whereas the BT474, JIMT-1 and MDA-MB-231 cells were maintained in DMEM. All culture media were supplemented with 10% fetal bovine serum and 1% penicillin/streptomycin. Cells were cultured at 37°C in a humidified incubator with 5% atmospheric CO_2.

Establishment of an ADCC-resistant cell line

We co-cultured 1×10^6 SKBR3 cells with 1×10^7 isolated healthy PBMCs for 4–9 h in medium containing 1–10 μg/ml trastuzumab. The cell mixture was incubated with CD45 Micro Beads, and CD45-positive PBMCs were removed with the MACS cell separation system (Miltenyi Biotec, Bergisch Gladbach, Germany) according to the manufacturer's instructions. The surviving SKBR3 cells were subsequently co-cultured several times with PBMCs in medium containing 1–10 μg/ml trastuzumab.

Cell cytotoxic assay

Cell cytotoxicity was measured with the LDH Cytotoxicity Test Kit (Wako, Osaka, Japan), the sensitivity of which is similar to that of the traditional Cr^{51} assay. In the ADCC assay, PBMCs were used as effector cells, whereas cancer cells were used as target cells. Trastuzumab (Chugai Pharmaceutical Co., Tokyo, Japan) and cetuximab (Merck Serono, Ltd., Darmstadt, Germany) were used as the treatment antibodies. In preliminary experiments of ADCC, the optimal ratio of effector to target was verified for each cell line (data not shown) and fixed at 20:1 unless otherwise indicated. In an antibody-independent cellular cytotoxicity (AICC) the effector-to-target ratio was at 10:1, 20:1 or 60:1. The cellular cytotoxicity was calculated with the following formula: % specific lysis = [(effector release − target release) − effector control release] − negative control / (positive control release − negative control release) × 100.

RNA-sequencing

RNA-sequencing analysis was performed with the Ion Proton System for next-generation sequencing (Life Technologies, Grand Island, NY). For each sample, 10 ng total RNA was reverse transcribed with the Ion AmpliSeq Transcriptome Human Gene Expression Kit (Life Technologies). We

eliminated all summarized gene counts other than those with raw counts over 10 reads per kilobase per million mapped reads.

Construction of *a short hairpin RNA plasmid and transfection*

The following short hairpin RNA (shRNA) sequence targeting *ATP6V1B1* (GenBank: NM_001692.3) was designed with the BLOCK-iT™ RNAi Designer (Invitrogen, Carlsbad, CA): ATP6V1B1 shRNA (5′-GGACCTGCTCTACCTGGAATTTTCAAGAGAAATTCCAGGTAGAGCAGGTCC-3′). Additionally, a scrambled control shRNA sequence was also generated (5′-GAGCGCCTTCTCTACGTAAGTTTCAAGAGAACTTACGTAGAGAAGGCGCTC-3′). The *ATP6V1B1* shRNA and scrambled control shRNA sequences were cloned into the pSIREN-retroQ retroviral vector. The recombinant plasmid DNA was purified with the Plasmid Midi kit (Qiagen, Hilden, Germany), and then used to transfect cells with ScreenFect™ A (Wako), FuGENE HD (Promega, Madison, WI), and Lipofectamine® 2000 (Thermo Fisher Scientific, Waltham, MA) transfection reagents. The resulting cells were selected with 1–2 μg/ml puromycin 2 days after transfection to establish stable knockdown lines.

RNA isolation and quantitative real-time PCR

Total RNA was extracted with TRIzol reagent (Ambion, Life Technologies), after which 1 μg total RNA was reverse transcribed with SuperScript III (Invitrogen) to synthesize cDNA. Next, 4 ng cDNA was used as the template for a quantitative real-time (qRT)-PCR amplification with the LightCycler® real-time PCR system (Roche, Basel, Switzerland). Relative gene expression levels were calculated according to the ΔΔCt method. The following primers were used for the qRT-PCR analysis: ATP6V1B1: (forward) 5′-GAATGGAACCATGGGGAAC-3′ and (reverse) 5′-GGTGATGATCCGCTCGAT-3′; SLC4A11: (forward) 5′-GAGGTTCGGTTCGTCATCC-3′ and (reverse) 5′-GAGAACATGGTGGCAAACG-3′; SLC16A3: (forward) 5′-AGACTCGGGGGTGGACTT-3′ and (reverse) 5′-ACCACCTCCCCGTTTTTCT-3′; SLC9A7: (forward) 5′-GAAGGTTGTGGTCCTTTGCT-3′ and (reverse) 5′-TTAATTACCTGCTACGGAAACCA-3′; ATP2B1: (forward) 5′-TATTGCTCAAGTGAAATATGGTGAT-3′ and (reverse) 5′-CAATTTTAAGATCGTTGCCTTGA-3′; ATP2A3: (forward) 5′-GAAGCAATTCATCCGCTACC-3′ and (reverse) 5′-CAGAATTGCCGTGAGGAAG-3′; GAPDH: (forward) 5′-AGCCACATCGCTCAGACAC-3′ and (reverse) 5′-GCCCAATACGACCAAATCC-3′.

Bafilomycin treatment

Bafilomycin A1 (Sigma-Aldrich, St Louis, MO) was dissolved in dimethyl sulfoxide as a stock solution and stored at −20°C. Cells were cultured and treated with 400 nM bafilomycin A1 for 2 h prior to the ADCC assay.

Establishment of ATP6V1B1-knockout cells

Open-access CRISPR design tools (http://crispr.mit.edu/) were used to design the guide RNA (gRNA) targeting *ATP6V1B1* exon 3. Annealed oligonucleotides were ligated into the gRNA cloning vector (Addgene, Watertown, MA), which was a gift from Motoji Mashimo (Osaka University, Osaka, Japan). The resulting recombinant plasmid was sequenced to confirm that the ligation was successful. We added 4×10^5 SKBR3 cells to a 6-well plate containing antibiotic-free medium. The plate was incubated overnight, after which the cells were transfected with 1.25 μg gRNA vector and 1.25 μg hCas9 vector (Addgene), which was a gift from Motoji Mashimo (Osaka University), with the ScreenFect™ A transfection reagent (Wako). Single-cell colonies were isolated for subsequent DNA extraction, protein extraction, and cryopreservation. The following PCR primers spanning potential deletion sites were designed: (forward) 5′-AGGGACTTTGCCTCCAGTCT-3′ and (reverse) 5′-GACCATTTCCTGCCTTCAGA-3′). PCR amplification products with deletions were

selected for subsequent analysis. The remaining clones were screened with the Surveyor Nuclease Assay (Integrated DNA Technologies, Coralville, IA). Mutations were confirmed by sequencing.

Western blotting

The cultured cells were washed twice with ice-cold PBS and lysed on ice in RBD lysis buffer containing a freshly added protease inhibitor cocktail. After a 10-min incubation on ice, the cell lysate was collected by centrifugation at 13,000 × g for 10 min at 0°C. The total protein concentration was determined with a Protein Assay Bicinchoninate Kit (Nacalai Tesque, Kyoto, Japan), after which the total protein (30 μg/lane) was separated by SDS-PAGE. The proteins were transferred to a PVDF membrane, blocked with Blocking One (Nacalai Tesque), and probed with an anti-ATP6V1B1 antibody (Atlas Antibodies, Bromma, Sweden). The primary antibody was then visualized with horseradish peroxidase-conjugated secondary antibodies and the LAS 4000 imaging system (GE Healthcare, Buckinghamshire, England).

Cell proliferation assay

Cancer cells ($4x10^3$/100μl medium) of each cell line are seeded in a 96-well plate and are incubated at 37°C with 5% atmospheric CO_2 for 24, 48, 72, 96, and 144 h. Cell proliferation was measured

with the WST8 assay (Dojindo Laboratories, Kumamoto, Japan) or MTS assay (Abcam, Cambridge, UK) according to the manufacturer's instruction. The absorbance (450 nm/ WST assay, 490nm/MTS assay) was measured with a microplate reader.

Flow cytometry

A multicolor flow cytometry analysis was performed with the FACS Canto system (BD Biosciences, San Jose, CA) and the following antibodies: PE-conjugated anti-human EGFR (BioLegend, San Diego, CA), APC-conjugated anti-human CD340 (ErbB2/HER2) (BioLegend), APC-conjugated anti-human ErbB3/HER3 (BioLegend), APC-conjugated anti-human ErbB4/HER4 (R&D), FITC-conjugated anti-human CD107a (BioLegend), PE-conjugated anti-human CD56 (BioLegend), FITC-conjugated anti-human granzyme A (BD Biosciences), and FITC-conjugated anti-human granzyme B (BioLegend).

Granzyme B staining of target cells

Individual 15-mm micro cover glasses were set onto a 12-well plate, after which 1×10^5 SKBR3 and *ATP6V1B1*-knockout (KO) cells were added to each well 2 days before the assay. The PBMCs of healthy volunteers were isolated and 8×10^6 effecter cells and 1 μg/ml trastuzumab were added to

each well containing cancer cells. The ADCC reactions were initiated with an effector-to-target ratio of 80:1. At 15, 30, and 45 min after initiating the ADCC reaction, the medium was removed, the cover glasses were washed with PBS, and cells were fixed for 20 min in PBS with 4% paraformaldehyde. Cells were then washed with PBS and permeabilized for 10 min in PBS with 0.5% Triton X-100. After two washes with PBS, the cover glasses were immersed in a PBS buffer with 1% BSA for 20 min, washed once with PBS, and incubated for 1 h at room temperature in PBS buffer with 1% BSA and the primary antibody (mouse anti-human GzmB, clone GB11; GeneTex). Cells were then washed three times with PBS and incubated for 1 h at room temperature in PBS buffer with 1% BSA, goat Alexa Fluor 488-conjugated secondary antibodies (Invitrogen), and DAPI (Dojindo). Cells were then washed three times with PBS, mounted in Calbiochem Mowiol reagent (Merck, Darmstadt, Germany), and examined with the Eclipse Ti microscope (Nikon, Tokyo, Japan).

Measurement of the intracellular pH of live cells

We added 10,000 cells to each well of a 96-well black plate 3 days before an assay. After removing the medium and washing twice with LCIS (Live Cell Imaging Solution, invitrogen), the cells were treated with 3 μM BCECF-AM (Dojindo Laboratories, Kumamoto, Japan) at 37°C for 30 min. The cells were then washed thoroughly with LCIS and analyzed with the Flex Station 3

spectrophotometer (Molecular Devices, Tokyo, Japan) at excitation/emission wavelengths of 490 nm/530 nm and 440 nm/530 nm. A calibration curve was prepared based on the incubation of cells in calibration buffers (pH adjusted to 5.5–7.5) containing 10 μM valinomycin and nigericin (Intracellular pH Calibration Buffer Kit; Thermo Fisher Scientific).

Cell block preparation

Formalin-fixed and paraffin-embedded (FFPE) cell blocks of breast cancer cell lines SKBR3, ADCC-resistant SKBR3 cell line (SKr), and *SK-V1B1*-KO were prepared. Specifically, each cell suspension (> 5×10^6 cells) was centrifuged at 600 × g for 3 min. The resulting cell pellets were fixed in 10% neutral-buffered formalin for 24 h and then embedded in paraffin. The FFPE blocks were cut into 4-μm thick sections.

Human tissue sample preparation

We prepared FFPE cell blocks for tissue samples collected from HER2+ early-stage breast cancer patients of the Department of Breast Surgery, Kyoto University Hospital who received neoadjuvant chemotherapy including trastuzumab, but did not exhibit a pathological complete response. Written informed consent was obtained from all patients prior to collecting tissue samples. All study

protocols were approved by the Ethics Committee for Clinical Research of Kyoto University Hospital (authorization number G424).

Immunohistochemistry

Immunohistochemical analyses of samples were completed with the BOND-RX automated immunostainer (Leica Biosystems, Newcastle, UK) and the BOND Polymer Refine Detection kit (Leica Biosystems, Wetzlar, Germany). Epitope retrieval was performed with the immunostainer by heating the FFPE sections in BOND Epitope Retrieval Solution 2 (Leica Biosystems) at 100°C for 20 min. All other incubations were performed at room temperature. Anti-ATP6V1B1 mouse monoclonal antibody (clone 1H6; Novus Biological, Littleton, CO), which served as the primary antibody, was diluted 1:200 (approximately 4 μg/ml). Mouse IgG1 (Dako, Glostrup, Denmark) was used as the negative control under the same conditions.

Statistical analysis

The significance of differences between groups was determined by unpaired two-tailed Student's t-test or the Mann–Whitney test. Results were considered statistically significant at $p < 0.05$. Data were analyzed with STATA version 13.0.

Data Availability

The datasets generated during and analyzed during the current study are not publicly available due to protecting participant confidentiality but are available from the corresponding author on reasonable request.

Results

Expression of ATP6V1B1 was downregulated in ADCC-resistant cell line

We established a trastuzumab-mediated ADCC-resistant SKBR3 cell line (SKr) to investigate the molecules in cancer cells involved in the acquired resistance. After seven passages, which required approximately 6 months, cytotoxicity was measured with a conventional ADCC assay with various trastuzumab concentrations. The cytotoxicity was lower for the ADCC-resistant SKBR3 cells than for the wild-type SKBR3 cells (Fig. 1a). The abundance of HER family receptors and cell proliferation were identical between the wild-type SKBR3 and ADCC-resistant SKBR3 cells (Supplementary Fig. 1a and b). And, ADCC-resistant SKBR3 cells were not resistant to trastuzumab itself (Supplementary Fig. 1c). We subsequently compared the gene expression levels between the wild-type and ADCC-resistant SKBR3 cells by RNA-sequencing. An analysis of the intracellular pH-regulating genes revealed that six genes (*ATP6V1B1*, *SLC16A3*, *SLC4A11*, *SLC9A7*, *ATP2B1*, and *ATP2A3*) were differentially expressed in ADCC-resistant SKBR3 cells relative to the corresponding expression levels in the wild-type cells, with fold-changes of < 0.66 or > 1.5 (Supplementary Table 1). The expression levels of these six genes were further evaluated with a qRT-PCR assay, which indicated that *ATP6V1B1* and *SLC4A11* expression levels were remarkably downregulated in the ADCC-resistant cells (Fig. 1b). Because it was previously reported that

SLC4A11 (a member of the SLC4 family of HCO_3^- transporters) does not affect intracellular pH[17], we focused on ATP6V1B1 in the present study. The abundance of the ATP6V1B1 protein was lower in the ADCC-resistant cells than in the wild-type SKBR3 cells according to western blot and immunohistochemistry results (Supplementary Fig. 1c and d). The *ATP6V1B1* gene is one of 24 genes encoding at least 13 subunits of V-ATPase. The B subunit is important for ATP hydrolysis, which drives the proton transport associated with V-ATPase. Thus, we focused on the *ATP6V1B1* gene in subsequent experiments.

ADCC was suppressed in ATP6V1B1-knockdown SKBR3 and NCI-N87 cells

To clarify the effect of ATP6V1B1 on trastuzumab-mediated ADCC, we knocked down the *ATP6V1B1* gene in SKBR3, BT474 and NCI-N 87 cells and found ATP6V1B1 of SKBR3 and NCI-N87 was knocked down successfully but not BT474 cells due to lack of ability of shRNA induction. The susceptibility to ADCC of the *ATP6V1B1*-knockdown SKBR3 and NCI-N87 cells ($SKBR3^{shATP6V1B1}$ and $NCI\text{-}N87^{shATP6V1B1}$) was significantly suppressed compared with the cells with the scrambled control shRNA ($SKBR3^{shNC}$ and $NCI\text{-}N87^{shNC}$) (Fig. 2a). The cytotoxicities of $SKBR3^{shATP6V1B1}$ and $SKBR3^{shNC}$ cells were 30.0% and 42.4%, respectively, in the presence of 1 μg/ml trastuzumab, whereas the cytotoxicities of $NCI\text{-}N87^{shATP6V1B1}$ and $NCI\text{-}N87^{shNC}$ cells were

10.1% and 20.4%, respectively, in the presence of 0.1 μg/ml trastuzumab. The qRT-PCR results indicated that the *ATP6V1B1* expression levels were 40% and 80% lower in the SKBR3 and NCI-N87 cells expressing *ATP6V1B1* shRNA, respectively, than in the cells with the scrambled control shRNA (Supplementary Fig. 2a and b). In order to confirm the role of V-ATPase in ADCC activity, because *ATP6V1B1* is not expressed in MDA-MB-231 cells, *ATP6V1B2* was knocked down, and the ADCC in the presence of cetuximab was analyzed. The susceptibility to ADCC of the *ATP6V1B2*-knockdown MDA-MB-231 cells (MDA-MB-231^{shATP6V1B2}) was significantly suppressed compared with the cells with the scrambled control shRNA (MDA-MB-231^{shNC}) (Supplementary Fig. 2c and d). The cytotoxicities of MDA-MB-231^{shATP6V1B2} and MDA-MB-231^{shNC} cells were 5.3% and 11.0%, respectively, in the presence of 0.1 μg/ml cetuximab. Furthermore, an analysis of the ADCC in SKBR3 and BT474 cells treated with bafilomycin A1, which is a specific inhibitor of V-ATPase, revealed a significant decrease in cytotoxicity (Fig. 2c and d). The cytotoxicities of the SKBR3^{untreated} and SKBR3^{Baf} cells were 34.0% and 19.6%, respectively, whereas the cytotoxicities of the BT474^{untreated} and BT474^{Baf} cells were 36.0% and 19.6%, respectively, in the presence of 1 μg/ml trastuzumab.

ADCC decreased in ATP6V1B1-KO cells

To further determine whether V-ATPase contributes to ADCC, we used the CRISPR-Cas9 system to generate *ATP6V1B1*-KO SKBR3 cells. Western blot and immunohistochemistry results confirmed the lack of ATP6V1B1 in a cell culture derived from a single cell (Fig. 3a and b). However, there were no differences in cell proliferation and the abundance of HER family proteins between the wild-type SKBR3 and *ATP6V1B1*-KO cells (Supplementary Fig. 2a and b). The ADCC was considerably lower in the *ATP6V1B1*-KO cells than in the wild-type SKBR3 cells in the presence of 0.1 μg/ml of trastuzumab (19.8% and 55.6%, respectively) (Fig. 3c). We also established *ATP6V1B1*-KO JIMT-1 (another HER2+ human breast cancer cell line) cells. Similar to the SKBR3 cells, in JIMT-1 cells, ADCC was significantly lower in *ATP6V1B1*-KO cells than in wild-type JIMT-1 cells in the presence of 1 μg/ml trastuzumab (39.7% and 19.7%, respectively) (Fig. 3d).

The intracellular environment of ATP6V1B1-KO cells was more acidic than that of wild-type cancer cells

A neutral environment (pH 7.5) is necessary for granzyme bioactivity. We speculated that impaired pH regulation in cancer cells due to abnormal V-ATPase functions may adversely affect the ability of NK cells to induce the apoptosis of cancer cells. Therefore, we compared the intracellular pH of wild-type SKBR3 and *ATP6V1B1*-KO cells. Following treatment with BCECF-AM, the fluorescence

intensity was measured with a microplate reader, and the pH was calculated. The intracellular pH of *ATP6V1B1*-KO cells was 6.9, whereas that of wild-type SKBR3 cells was 7.5 (Fig. 4a). These results suggested that the cytoplasm of *ATP6V1B1*-KO cells may not be suitable for granzyme bioactivity. Similar to SKBR3-*ATP6V1B1*-KO cells, SKr cells and JIMT-1-*ATP6V1B1*-KO cells also showed decreased intracellular pH compared to wild type (7.4 and 6.9, 7.6 and 7.2, respectively) (Fig. 4b and 4c).

Granzyme B accumulated in the acidic cytoplasm of ATP6V1B1-KO cancer cells during the ADCC reaction

To evaluate the effect of a lack of ATP6V1B1 on the amount of granzymes released from NK cells during the ADCC reaction, we co-stained cells to detect CD107a and CD56, which reflected the granule content released from NK cells, at 15 min after the ADCC reaction was initiated. There were no differences between the wild-type SKBR3 and *ATP6V1B1*-KO cells regarding the CD56-positive and CD107a-positive regions (Fig. 5a). Thus, the lack of ATP6V1B1 did not appear to affect the amount of granzyme released from NK cells during the ADCC reaction. We next applied flow cytometry to analyze the amounts of granzymes A and B in wild-type SKBR3 and *ATP6V1B1*-KO cells at 15 min after the ADCC reaction was initiated. Interestingly, the intracellular amounts of

granzymes were significantly higher in *ATP6V1B1*-KO cells (9.1% granzyme A and 15.6% granzyme B) than in wild-type SKBR3 cells (1.2% granzyme A and 5.4% granzyme B) (Fig. 5b). We also confirmed that the intracellular amounts of granzymes were higher in *ATP6V1B1*-KO JIMT-1 cells (5.2% granzyme A and 20.6% granzyme B) than in wild-type JIMT-1 cells (3.0% granzyme A and 12.1% granzyme B) (Fig. 5c). Additionally, to visualize the intracellular dynamics of granzyme B during the ADCC reaction, the granzyme B of wild-type SKBR3 and *ATP6V1B1*-KO cells was stained at 15, 30, and 45 min after the ADCC reaction was initiated. The granzyme B taken up by cells was degraded in the cytoplasm and nucleus of wild-type SKBR3 cells, but accumulated in the cytoplasm and nucleus of *ATP6V1B1*-KO cells (Fig. 5d). These observations suggest that the decreased intracellular pH of *ATP6V1B1*-KO cells may have inhibited the ability of granzyme B to mediate the apoptosis of the cancer cells.

AICC decreased in ATP6V1B1-KO cells

Similar to ADCC, AICC involves the release of granzymes from NK cells. We predicted that a lack of ATP6V1B1 affects AICC similar to how it affects ADCC. To test this hypothesis, we induced the AICC reaction with effector-to-target ratios of 10:1, 20:1, and 60:1. The cytotoxicity of the *ATP6V1B1*-KO cells was lower than that of the wild-type SKBR3 cells for each effector-to-target

ratio (12.5% and 41.2% for the 10:1 effector-to-target ratio, 9.5% and 46.5% for the 20:1 effector-to-target ratio, and 7.3% and 50.7% for the 60:1 effector-to-target ratio, respectively) (Fig. 6) although JIMT-1 cells are not susceptible to NK cell killing and difference of AICC activity was not shown between wild type and ATP6V1B1-KO JIMT-1 cells (Supplementary Fig 4).

The ATP6V1B1 expression level of the residual tumor cells may decrease after neoadjuvant chemotherapy including trastuzumab

To explore whether the *ATP6V1B1* expression level is associated with clinical outcomes, we completed an immunohistochemical analysis of *ATP6V1B1* expression in samples collected from 14 patients with HER2+ breast cancer who received neoadjuvant chemotherapy including trastuzumab, but did not exhibit a pathological complete response (Table 1). Breast cancer tissues were stained to detect ATP6V1B1, after which the staining intensity was compared between the pre- and post-chemotherapy biopsy samples. The staining intensity was scored independently by three people (MN, TK, and TS) based on the following scale: 0, no staining; 1, partial staining; 2, overall weak staining; and 3, overall strong staining (Fig. 7a). The resulting scores were averaged. The staining intensities tended to be lower for the post-chemotherapy samples than for the pre-chemotherapy samples (0.67 and 1.67, respectively) (Fig. 7b). This observation suggested that in the residual tumor

cells, which were likely resistant to chemotherapy, *ATP6V1B1* expression levels decreased from the pre-chemotherapy levels, and these results are consistent with in vitro experimental results.

Discussion

Granzymes are essential for the targeted effects of ADCC. Specifically, granzymes released from immune cells induce targeted cell death through a caspase or non-caspase pathway[18,19,20]. The optimal pH for granzyme bioactivity is 7.5[16]. In this study, we demonstrated that granzyme bioactivity is suppressed by downregulating *ATP6V1B1* expression and decreasing intracellular pH. This suggests that decreased intracellular pH may be correlated with the antitumor effects of other antibody-targeted therapies that elicit ADCC, including the use of molecular agents targeting CD20. More importantly, considering that granzymes are critical for cytotoxic activities targeting cancer cells, increased acidity may contribute to the suppression of the antitumor effects of NK cells and cytotoxic T lymphocytes.

Granzyme-mediated cytotoxicity of NK cells against cancer cells is common not only to ADCC but also to AICC. As shown in Fig 6a, AICC activity was also reduced in the ATP6V1B1-KO cell line. AICC was also shown in Fig 2a, 2d, 3c, and sFig2c at a trastuzumab concentration of 0 mg/ml, and showed the same suppressive reaction with V-ATPase downregulation as ADCC. These results are

consistent with our hypothesis that the antitumor effect is suppressed by suppressing the activation of granzyme by pH acidification. We believe that the results described herein may be of some help in elucidating the mechanism responsible for the weak therapeutic effects of immune checkpoint inhibitors.

We focused on V-ATPase as a molecule that controls intracellular pH. This enzyme is usually localized to the plasma membrane as well as the vesicular membranes of organelles, such as endosomes and lysosomes, where it helps maintain an acidic environment inside the membrane[21]. V-ATPase is inhibited by disrupting the production of ATP6V1B1, which is a V-ATPase subunit responsible for ATP hydrolysis[22], and thus decreases the intracellular pH of *ATP6V1B1*-KO cells to 6.9 (Fig. 4a). This phenomenon is likely the result of the cytoplasmic accumulation of protons that would normally be transferred by V-ATPase to organelles or the extracellular space.

The ideal pH for granzyme bioactivity is 7.5, and deviations from this optimal pH adversely affect granzyme functions. Analyses of granzyme dynamics in cells during the ADCC reaction revealed that intracellular granzymes were undetectable at 45 min after the ADCC reaction was initiated in wild-type SKBR3 cells with an intracellular pH of 7.5. In contrast, in *ATP6V1B1*-KO cells with an intracellular pH of 6.9, granzymes were still detected in the cytoplasm at 45 min after the initiation of the ADCC reaction（Fig. 5c). These observations imply that granzymes are inactive in

ATP6V1B1-KO cells because of an unsuitably acidic intracellular environment and are present as nonfunctional proteases that are not degraded, although they are normally degraded after functionally activated.

Because of the difficulty in developing experimental animal models of HER2+ breast cancer with an autologous immune system for elucidating the immune reaction by regulating the production of V-ATPase, we evaluated *ATP6V1B1* expression with pre-operative and surgically resected clinical samples from HER2+ breast cancer patients who received neoadjuvant systemic therapy including trastuzumab. Although the results were preliminary, we observed that the staining intensity, which represented the ATP6V1B1 content, decreased in the residual tumor cells resistant to the trastuzumab-containing therapy. This phenomenon partly reflects our experimental findings, suggesting that ATP6V1B1 is important for ADCC. However, because in this study the number of cases is limited, it should be cautious in the interpretation of this result. We also explored the possibility of a therapeutic effect predictor of ATP6V1B1 and analyzed the correlation between the staining intensity of ATP6V1B1 in biopsy samples and the therapeutic effect (Supplementary Fig. 5). It was suggested that chemotherapy may be effective in cases with high staining intensity (Grade 2 and 3) in biopsy samples, but there was no correlation with the effect of chemotherapy in cases with low staining intensity (Grade 0 and 1). Therefore, it was suggested that ATP6V1B1 is not a predictor

of chemotherapy effect but one of the molecules involved in the resistance mechanism of chemotherapy in clinical samples. We will continue to analyze large-scale clinical samples as a future task and will elucidate this series of phenomena.

We acknowledge that this study has limitations. It is important to note that the B subunit consists of two subunits, B1 and B2[23]. Additionally, B1 is not produced in all cancer cells, and its distribution may vary in each cancer cell. We screened a wide range of cell lines, including other carcinomas, that had an ADCC response and also had a B1 subunit, and tried to prove that these responses were common reaction. Among several cell lines, JIMT-1 cells were confirmed to be Her2-positive breast cancer cells with B1 subunit and ADCC reaction. We established *ATP6V1B1*-KO cells of JIMT-1 cells. It was confirmed that a series of experimental results such as ADCC reaction, intracellular pH, and intracellular amounts of granzymes in JIMT-1-*ATP6V1B1*-KO cells had the same tendency as that of SKBR3-*ATP6V1B1*-KO cells. In order to further generalize this phenomenon in different cell lines, it is necessary to verify other subunits including B2 and A subunits. Another limitation is that these series of reactions were not confirmed in vivo. Although it may be possible to make xenografts using JIMT-1 cells, SKBR3 did not grow in vivo. Further investigation and efforts in vivo experiment may be needed.

In addition to V-ATPase, there are various pH-regulating molecules, including carbonate dehydrogenase, Na^+/HCO_3^- co-transporters, Na^+/H^+ exchangers, monocarboxylic acid transporters, and ion exchangers[24]. It is conceivable that these molecules help control intracellular pH. In this study, we determined that the pH of the intracellular environment affects granzyme bioactivity and may influence the resistance to trastuzumab-mediated cytotoxicity related to immune mechanisms. For the purpose of predicting therapeutic effects and developing a novel treatment target aimed at reinforcing the effects or reversing resistance, we need to further explore the integrated functions of various pH-regulating genes to regulate the intracellular pH that may affect immune-mediated cellular cytotoxicity. We should also develop a novel method for measuring the intracellular pH of clinical samples in the future.

Acknowledgments

This research was supported by a grant from the Japan Society for the Promotion of Science through the KAKENHI Grant Numbers 24591901. We thank Keiko Sakamoto, Yuji Fukushima, Masashi Inoue and Sunao Tanaka for teaching experimental techniques and helping with the experiments.

References

1 Slamon, D. J. *et al.* Use of chemotherapy plus a monoclonal antibody against HER2 for metastatic breast cancer that overexpresses HER2. *The New England journal of medicine* **344**, 783-792, doi:10.1056/NEJM200103153441101 (2001).

2 D Cameron, MJ Piccart-Gebhart, RD Gelber, *et al.*11 years' follow-up of trastuzumab after adjuvant chemotherapy in HER2-positive early breast cancer: final analysis of the HERceptin Adjuvant (HERA) trial. Lancet, 389 (2017), pp. 1195-1205

3 Harari, D. & Yarden, Y. Molecular mechanisms underlying ErbB2/HER2 action in breast cancer. *Oncogene* **19**, 6102-6114, doi:10.1038/sj.onc.1203973 (2000).

4 Saez, R. *et al.* p95HER-2 predicts worse outcome in patients with HER-2-positive breast cancer. *Clin Cancer Res* **12**, 424-431, doi:10.1158/1078-0432.CCR-05-1807 (2006).

5 Scaltriti, M. *et al.* Expression of p95HER2, a truncated form of the HER2 receptor, and response to anti-HER2 therapies in breast cancer. *Journal of the National Cancer Institute* **99**, 628-638, doi:10.1093/jnci/djk134 (2007)

6 Nagy, P. *et al.* Decreased accessibility and lack of activation of ErbB2 in JIMT-1, a herceptin-resistant, MUC4-expressing breast cancer cell line. *Cancer Res* **65**, 473-482 (2005).

7 Wang, Y. *et al.* Inhibition of insulin-like growth factor-I receptor (IGF-IR) signaling and tumor cell growth by a fully human neutralizing anti-IGF-IR antibody. *Mol Cancer Ther* **4**, 1214-1221, doi:10.1158/1535-7163.MCT-05-0048 (2005).

8 Nagata, Y. *et al.* PTEN activation contributes to tumor inhibition by trastuzumab, and loss of PTEN predicts trastuzumab resistance in patients. *Cancer Cell* **6**, 117-127, doi:10.1016/j.ccr.2004.06.022

9 Clynes RA, Towers TL, Presta LG, Ravetch JV. Inhibitory Fc receptors modulate in vivo cytotoxicity against tumor targets. Nature medicine **2000**;6:443-6

10 Florian Reim, et al. Immunoselection of Breast and Ovarian Cancer Cells with Trastuzumab and Natural Killer Cells: Selective Escape of $CD44^{high}/CD24^{low}/HER2^{low}$ Breast Cance Stem Cells. Cancer Res 2009; doi: 10.1158/0008-5472.CAN-09-0834

11 Scaltriti M, et al. Lapatinib, a HER2 tyrosine kinase inhibitor, induces stabilization and accumulation of HER2 and potentiates trastuzumab-dependent cell cytotoxicity. Oncogene 2009; doi: 10.1038/onc.2008.432.

12 Roca L, et al. Correlation of HER2, FCGR2A, and FCGR3A gene polymorphisms with trastuzumab related cardiac toxicity and efficacy in a subgroup of patients from UNICANCER-

PACS 04 trial. Breast Cancer Res Treat. 2013 Jun;139(3):789-800. doi: 10.1007/s10549-013-2587-x.

13 Tamura, K. *et al*. FcγR2A and 3A polymorphisms predict clinical outcome of trastuzumab in both neoadjuvant and metastatic settings in patients with HER2-positive breast cancer. *Ann. Oncol.***22**, 1302–1307 (2011).

14 Thiery, J. *et al.* Perforin pores in the endosomal membrane trigger the release of endocytosed granzyme B into the cytosol of target cells. *Nature immunology* **12**, 770-777, doi:10.1038/ni.2050 (2011).

15 Henkart, P. A., Berrebi, G. A., Takayama, H., Munger, W. E. & Sitkovsky, M. V. Biochemical and functional properties of serine esterases in acidic cytoplasmic granules of cytotoxic T lymphocytes. *J Immunol* **139**, 2398-2405 (1987).

16 Breton, S. & Brown, D. Regulation of luminal acidification by the V-ATPase. *Physiology (Bethesda)* **28**, 318-329, doi:10.1152/physiol.00007.2013 (2013).

17 Jalimarada, S. S., Ogando, D. G., Vithana, E. N. & Bonanno, J. A. Ion transport function of SLC4A11 in corneal endothelium. *Invest Ophthalmol Vis Sci* **54**, 4330-4340, doi:10.1167/iovs.13-11929 (2013).

18 Rousalova I, Krepela E. Granzyme B-induced apoptosis in cancer cells and its regulation (review). Int J Oncol **2010**;37:1361-78

19 Adrain C, Murphy BM, Martin SJ. Molecular ordering of the caspase activation cascade initiated by the cytotoxic T lymphocyte/natural killer (CTL/NK) protease granzyme B. The Journal of biological chemistry **2005**;280:4663-73

20 Martinvalet D, Dykxhoorn DM, Ferrini R, Lieberman J. Granzyme A cleaves a mitochondrial complex I protein to initiate caspase-independent cell death. Cell **2008**;133:681-92

21 Toei, M., Saum, R. & Forgac, M. Regulation and isoform function of the V-ATPases. *Biochemistry* **49**, 4715–4723 (2010).

22 Arai, S. *et al.* Rotation mechanism of Enterococcus hirae V1-ATPase based on asymmetric crystal structures. *Nature* **493**, 703-707, doi:10.1038/nature11778 (2013).

23 van Hille, B. *et al.* Heterogeneity of vacuolar H(+)-ATPase: differential expression of two human subunit B isoforms. *Biochem J* **303 (Pt 1)**, 191-198 (1994).

24 Casey, J. R., Grinstein, S. & Orlowski, J. Sensors and regulators of intracellular pH. *Nat Rev Mol Cell Biol* **11**, 50-61, doi:10.1038/nrm2820 (2010).

Figure 1

a

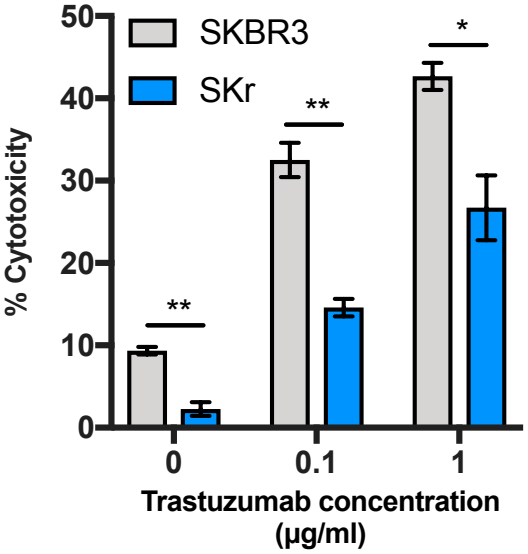
SKBR3
SKr
% Cytotoxicity
50
40
30
20
10
0
**
**
*
0
0.1
1
Trastuzumab concentration
(µg/ml)

b

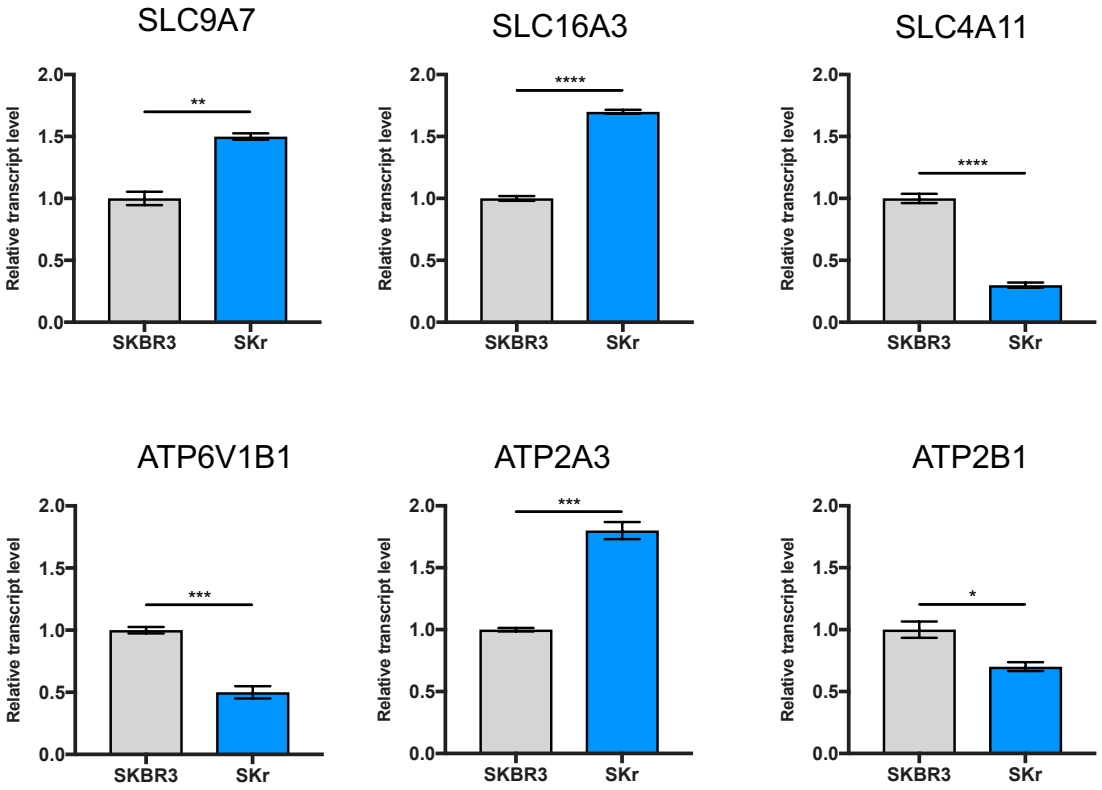
SLC9A7
SLC16A3
SLC4A11
ATP6V1B1
ATP2A3
ATP2B1
Relative transcript level
2.0
1.5
1.0
0.5
0.0
**
****
****
***
***
*
SKBR3
SKr

Figure 2

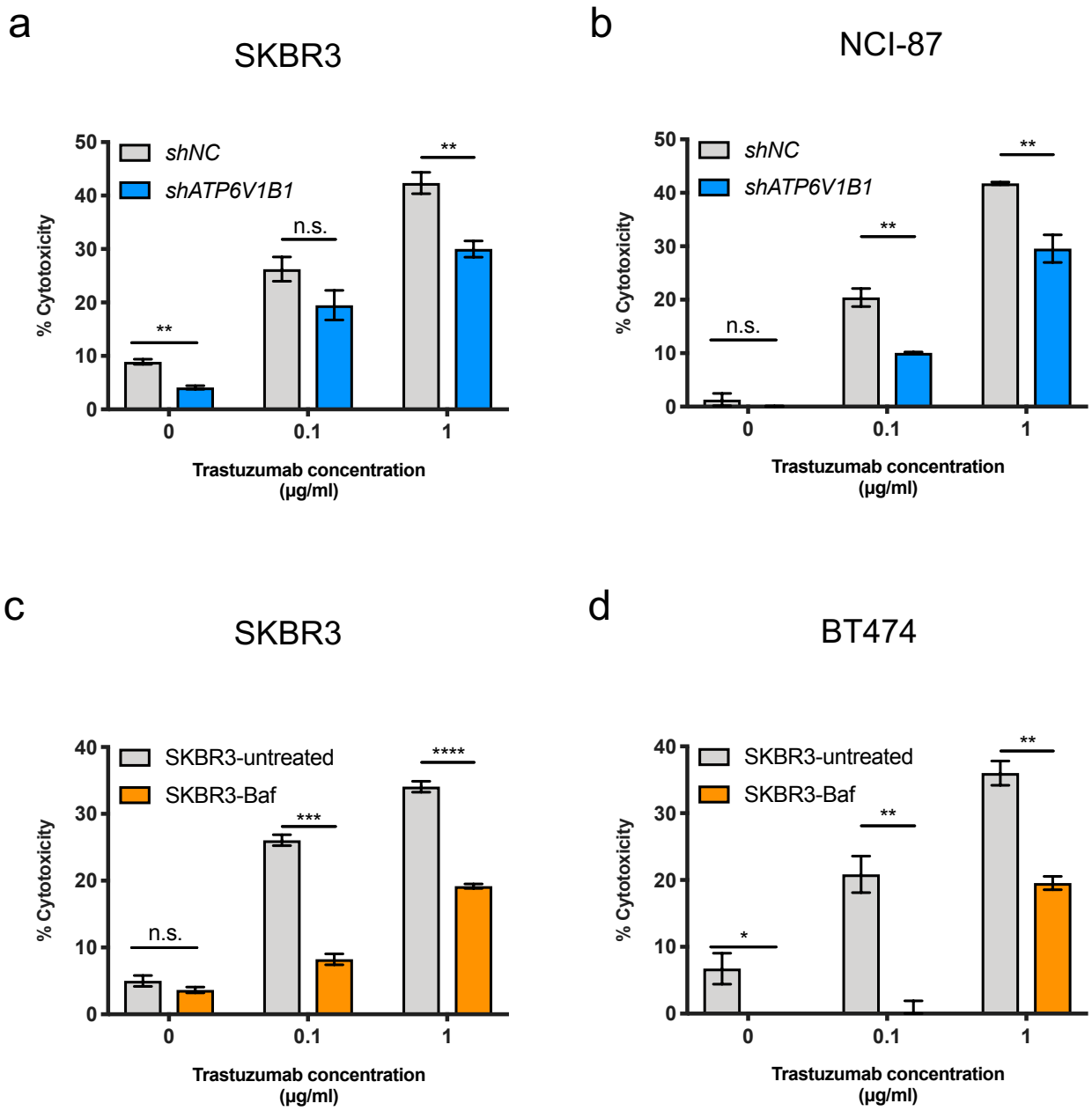
a
SKBR3
shNC
shATP6V1B1
% Cytotoxicity
50
40
30
20
10
0
**
n.s.
**
0
0.1
1
Trastuzumab concentration
(μg/ml)
b
NCI-87
shNC
shATP6V1B1
% Cytotoxicity
n.s.
**
**
0
0.1
1
Trastuzumab concentration
(μg/ml)
c
SKBR3
SKBR3-untreated
SKBR3-Baf
% Cytotoxicity
40
30
20
10
0
n.s.
***
****
0
0.1
1
Trastuzumab concentration
(μg/ml)
d
BT474
SKBR3-untreated
SKBR3-Baf
% Cytotoxicity
*
**
**
0
0.1
1
Trastuzumab concentration
(μg/ml)

Figure 3

a

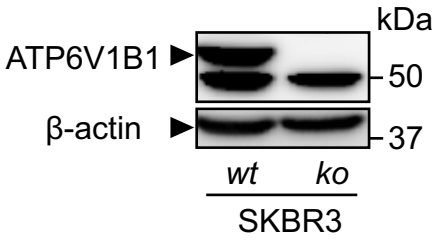

b

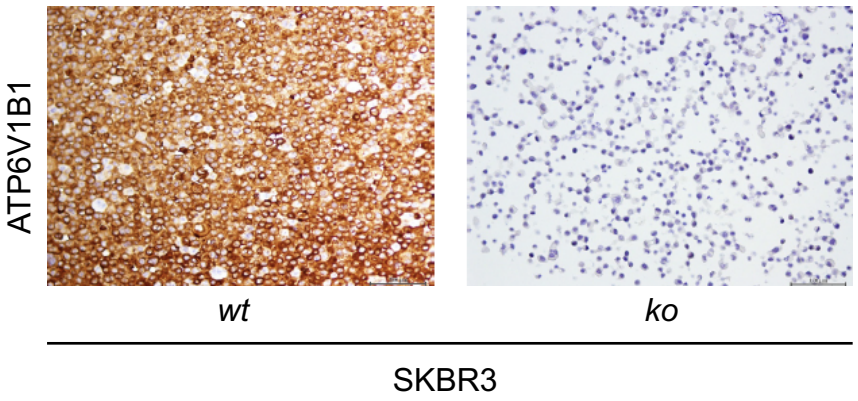

c

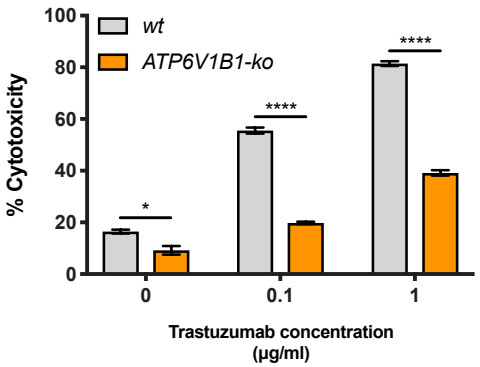

d

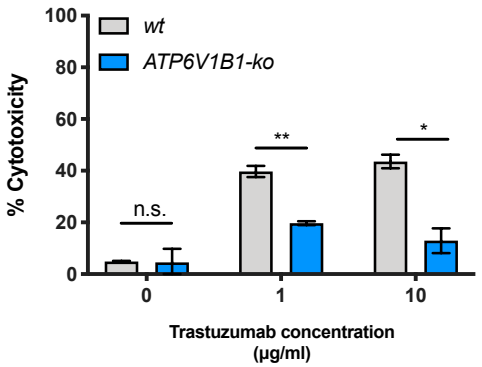

Figure 4

a

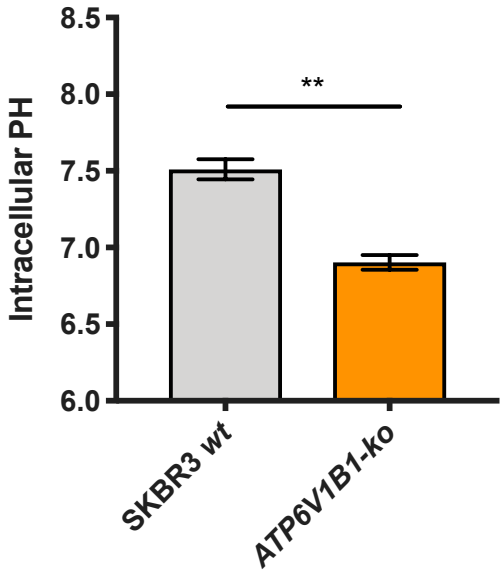
Intracellular PH
8.5
8.0
7.5
7.0
6.5
6.0
**
SKBR3 wt
ATP6V1B1-ko

b

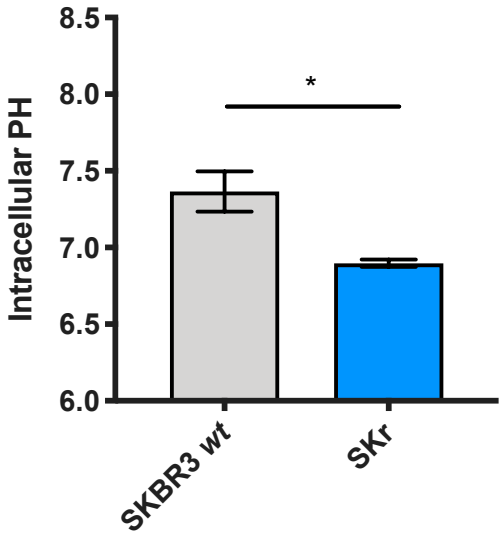
Intracellular PH
8.5
8.0
7.5
7.0
6.5
6.0
*
SKBR3 wt
SKr

c

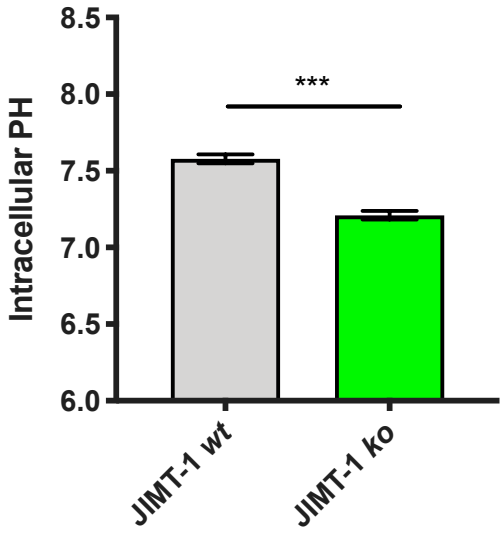
Intracellular PH
8.5
8.0
7.5
7.0
6.5
6.0
***
JIMT-1 wt
JIMT-1 ko

Figure 5

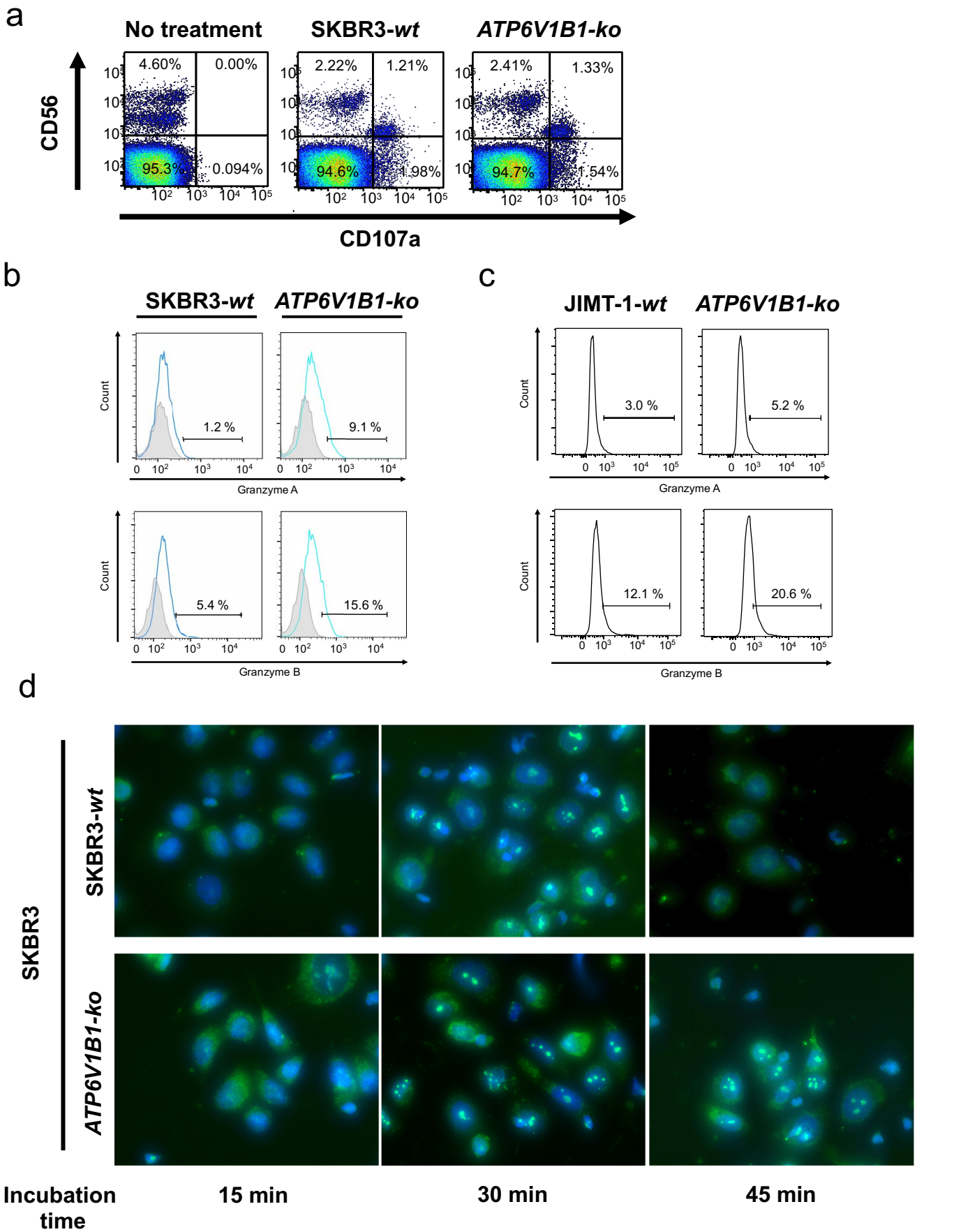
a
No treatment
SKBR3-wt
ATP6V1B1-ko
CD56
CD107a
4.60%
0.00%
95.3%
0.094%
2.22%
1.21%
94.6%
1.98%
2.41%
1.33%
94.7%
1.54%
b
SKBR3-wt
ATP6V1B1-ko
Count
1.2 %
9.1 %
Granzyme A
5.4 %
15.6 %
Granzyme B
c
JIMT-1-wt
ATP6V1B1-ko
Count
3.0 %
5.2 %
Granzyme A
12.1 %
20.6 %
Granzyme B
d
SKBR3
SKBR3-wt
ATP6V1B1-ko
Incubation time
15 min
30 min
45 min

Figure 6

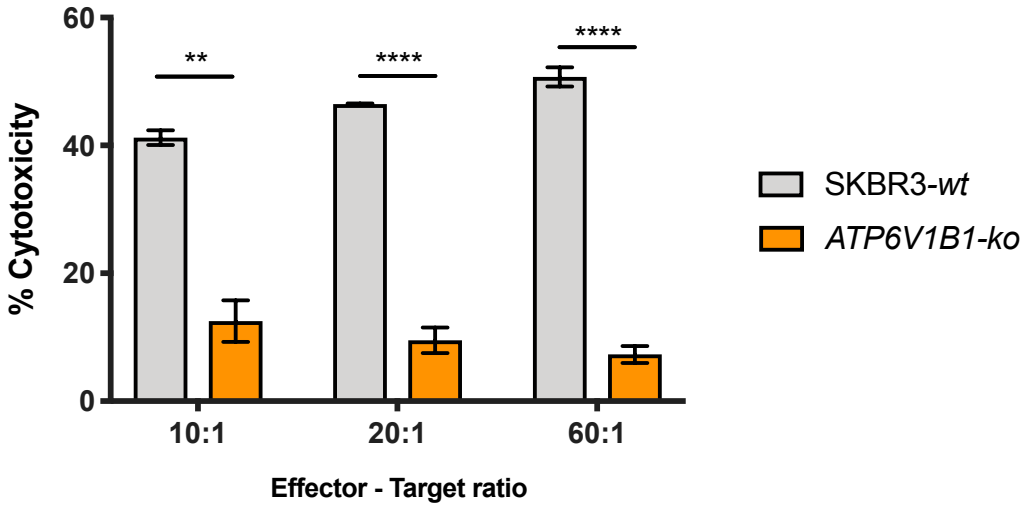
60
40
20
0
% Cytotoxicity
**
****
****
10:1
20:1
60:1
Effector - Target ratio
SKBR3-wt
ATP6V1B1-ko

Table 1 Patient characteristics

Tumor characteristics(N=14)		**No. of Patients(%)**
T stage	T1	3(21)
	T2	8(57)
	T3	3(21)
Clinical nodal stage	N0	2(14)
	N1	9(64)
	N1<	3(21)
ER status	positive	8(57)
	negative	6(43)
Therapeutic effect of neoadjuvant chemotherapy	grade1	5(36)
	grade2	9(64)

Figure 7

a

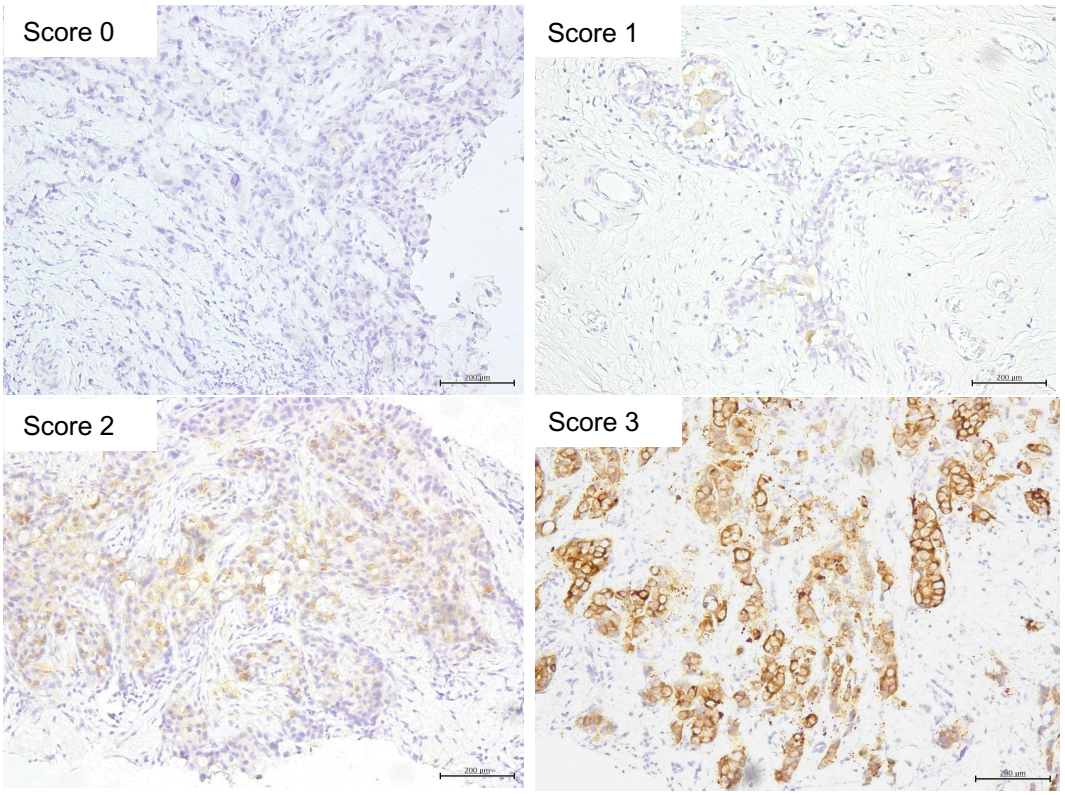
Score 0
Score 1
Score 2
Score 3

b

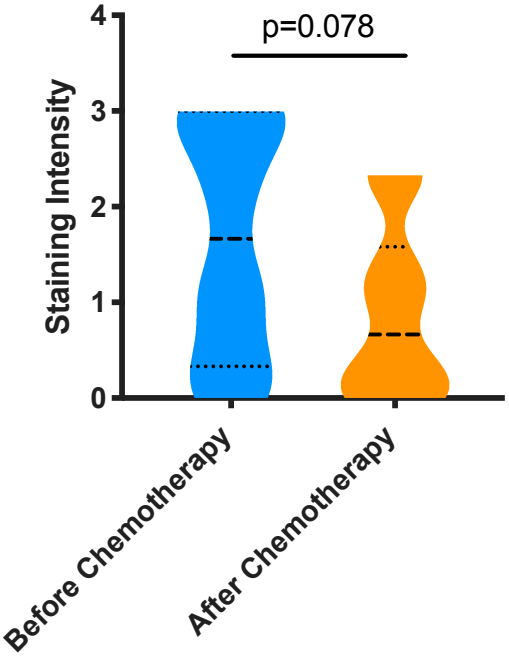
p=0.078
Staining Intensity
4
3
2
1
0
Before Chemotherapy
After Chemotherapy

Figure legends

Figure 1. A trastuzumab-mediated ADCC-resistant SKBR3 cell line was established by co-culturing SKBR3 cells with PBMCs for 4–9 h in a medium supplemented with 1–10 μg/ml trastuzumab. The surviving SKBR3 cells were then co-cultured several times with PBMCs in a medium with 1 μg/ml trastuzumab.

a) Cytotoxicitis of SKBR3 and ADCC-resistant SKBR3 cells (SKr) evaluated with the LDH assay. N = 3 for all experiments. *p < 0.05, **p < 0.01. **b)** A qRT-PCR assay was completed to analyze the expression levels of six genes that were differentially expressed between wild-type and ADCC-resistant SKBR3 cells according to RNA- sequencing data. Relative gene expression levels were calculated according to the ΔΔCt method. N = 3 for all experiments. *p < 0.05, **p < 0.01, ***p < 0.001, ****p< 0.0001. All graphs show mean ± SEM.

Figure 2. a and b) The ATP6V1B1 genes of SKBR3 and NCI-N 87 cells were knocked down, after which the ADCC was evaluated; **a)** The ADCC of SKBR3 and *ATP6V1B1*-knockdown; **b)** The ADCC of *ATP6V1B1*-knockdown NCI-N87 cells. N = 3 for all experiments. ns not significant. *p < 0.05 ,**p < 0.01. **c and d)** Changes to cytotoxicities after the bafilomycin A1 (specific inhibitor of

V-ATPase) treatment. Cells were cultured and treated with 400 nM bafilomycin A1 for 2 h prior to the ADCC assay. C. Wild-type SKBR3 cells vs bafilomycin-treated cells. D. Wild- type BT474 cells vs bafilomycin-treated cells. N = 3 for all experiments. *p < 0.05, **p < 0.01, ***p < 0.001, ****p < 0.0001, ns: not significant. All graphs show mean ± SEM

Figure 3. *ATP6V1B1-KO* SKBR3 cells lacked the ATP6V1B1 protein according to the western blot **(a)** and immunohistochemistry **(b)** results. **c)** An LDH assay was complete to compare the wild-type SKBR3 and *ATP6V1B1*-KO cells. The cytotoxicities of the wild-type SKBR3 and *ATP6V1B1*-KO cells were 55.6% and 19.8%, respectively, in the presence of 0.1 μg/ml trastuzumab ($p < 0.01$), and 81.5% and 39.1%, respectively, in the presence of 1 μg/ml trastuzumab ($p < 0.01$). N = 3 for all experiments. *p < 0.05, ****p < 0.0001. The graph shows mean ± SEM. **d)** An LDH assay was complete to compare the wild-type JIMT-1 and ATP6V1B1-KO cells. The cytotoxicities of the wild-type JIMT-1 and *ATP6V1B1*-KO cells were 39.7% and 19.7%, respectively, in the presence of 1 μg/ml trastuzumab ($p< 0.01$), and 43.6% and 12.9%, respectively, in the presence of 10 μg/ml trastuzumab ($p <0.05$). N = 3 for all experiments. **p < 0.01, *p < 0.05. The graph shows mean ± SEM.

Figure 4. Intracellular pH; **a)** wild-type SKBR3 and *ATP6V1B1*-KO cells **;b)** wild-type SKBR3 and SKr cells **;c)** wild-type JIMT-1 and *ATP6V1B1*-KO cells. The intracellular pH was determined after a treatment with BCECF-AM. Each bar represents the mean of three determinations. **p< 0.01, *p< 0.05., ***p< 0.001. The graph shows mean ± SEM.

Figure 5. a) PBMCs were co-stained to detect CD107a (marker of NK cell activity) and CD56 (NK cell marker), which reflected the granule content released by NK cells, at 15 min after the ADCC reaction was initiated. **b)** Wild-type SKBR3 cells (left) and *ATP6V1B1*-KO cells (right) were stained to detect granzymes A (upper) and B (lower) at 15 min after the ADCC reaction was initiated by flow cytometry. Grey is unstained control. **c)** Wild-type JIMT-1 cells (left) and *ATP6V1B1*-KO cells (right) were stained to detect granzymes A (upper) and B (lower) at 45 min after the ADCC reaction was initiated by flow cytometry **d)**. Microscopy analysis of wild-type SKBR3 cells (upper panels) and *ATP6V1B1*-KO cells (lower panels) with Alexa Fluor-labeled granzyme B during the ADCC reaction. Granzyme B of wild-type SKBR3 cells and *ATP6V1B1*-KO cells was stained at 15, 30, and 45 min after the ADCC reaction was initiated.

Figure 6. The AICC activities of wild-type SKBR3 cells and *ATP6V1B1*-KO cells were

evaluated with an LDH assay after culturing at an effector-to-target ratio of 10: 1, 20: 1, and 60: 1 for 4 hours. N = 3 for all experiments. **p < 0.01, ****p < 0.0001. The graph shows mean ± SEM. **p < 0.01, ****p < 0.0001. The graph shows mean ± SEM.

Figure 7. a) Staining intensity was classified based on the following scale: 0, no staining; 1, partial staining; 2, overall weak staining; and 3, overall strong staining. **b)** Distribution and intensity of the staining to detect ATP6V1B1 in human breast cancer biopsy samples (pre-chemotherapy) and samples collected during an operation (post-chemotherapy) (n = 14).

Figure legends

Table 1. Details regarding the patients diagnosed with HER2+ breast cancer who received neoadjuvant chemotherapy including trastuzumab, but did not exhibit a pathological complete response (n = 14).

Supplementary Table1

Gene	p-value	Fold change	*Gene*	p-value	Fold change
CA1	0.48292295	1.862385321	*SLC16A2*	0.107411431	0.804700143
CA2	0.034807717	3.103975535	*SLC16A4*	0.047687252	0.810576269
CA9	0.113892597	0.473741497	*SLC16A5*	0.021854982	0.287758831
CA11	0.030696284	3.536073059	*SLC16A6*	0.090835054	2.250672405
CA12	0.060658451	1.428846808	*SLC16A9*	0.304507666	0.699459094
CA13	0.175050167	5.703196347	*SLC16A10*	0.127700969	0.12335353
ATP6V1A	0.103449521	0.87463116	*SLC16A11*	0.676411647	0.504527814
ATP6V1B1	0.030586537	0.591936951	*SLC16A13*	0.956175113	1.035211268
ATP6V1B2	0.134801259	1.40505799	*NHE1(SLC9A1)*	0.329315453	1.095685987
ATP6V1C1	0.299839332	0.780451675	*NHE2(SLC9A2)*	0.557765427	0.92879151
ATP6V1C2	0.563804059	0.770875276	*NHE4(SLC9A4)*	0.926148686	0.861751152
ATP6V1D	0.999315863	1.000094564	*NHE5(SLC9A5)*	0.959191053	1.029473684
ATP6V1E1	0.002003579	1.135278533	*NHE6(SLC9A6)*	0.155248563	1.343474698
ATP6V1E2	0.057109928	5.013574661	*NHE7(SLC9A7)*	0.008473098	1.617715265
ATP6V1F	0.511408702	0.816633007	*NHE8(SLC9A8)*	0.006078466	1.216124568
ATP6V1G1	0.19407898	1.019436431	*AE2(SLC4A2)*	0.120883634	0.918284782
ATP6V1G2	0.834203657	0.900915241	*SLC26A1*	0.736491604	0.613293051
ATP6V1H	0.035512668	1.3161038	*SLC26A2*	0.047204785	0.354829381
ATP6V0A1	0.17788216	0.76755243	*SLC26A6*	0.644851439	0.899735923
ATP6V0A2	0.772714627	0.893532057	*SLC26A7*	0.422649731	0
TCIRG1	0.093144674	1.307660184	*SLC26A11*	0.336433703	0.910253429
ATP6V0A4	0.010147354	1.397843211	*ATP2B1*	0.180551971	0.591021198
ATP6V0D1	0.252606267	1.139290456	*ATP2B2*	0.070139828	5.864253394
ATP6V0E1	0.063640843	1.351515664	*ATP2B3*	0.422649731	0
ATP6V0C	0.071410689	1.127962703	*ATP2B4*	0.236134436	1.134856563
ATP6V0B	0.115470151	1.337628745	*CLCN1*	0.924047252	0.945454545
ATP6AP1	0.243728815	1.190668065	*CLCN2*	0.042611846	1.807813654
ATP6AP2	0.490591393	1.132425087	*CLCN3*	0.860702114	1.078673869
SLC4A3	0.232887628	0.57272203	*CLCN4*	0.089687519	0.150698856
SLC4A5	0.402656593	0.425874126	*CLCN5*	0.625457815	0.857859341
SLC4A7	0.356225016	0.814328358	*CLCN6*	0.626090431	0.956762625
SLC4A8	0.371553906	1.548406139	*CLCN7*	0.233435505	1.077989886
SLC4A10	0.564696542	0.288343558	*CLCNKA*	0.803118825	1.252120026
SLC4A11	0.009417537	0.394301813	*ATP2A1*	0.614849785	1.965328467
MCT1(SLC16A1)	0.012755356	2.904532305	*ATP2A2*	0.159491819	0.832593425
MCT3(SLC16A8)	0.422649731	0	*ATP2A3*	0.028599215	1.875724802
MCT4(SLC16A3)	0.051875002	1.811033587	*ATP2C1*	0.154420005	0.895964458
			ATP2C2	0.001071433	1.628114992

Supplementary Figure 1

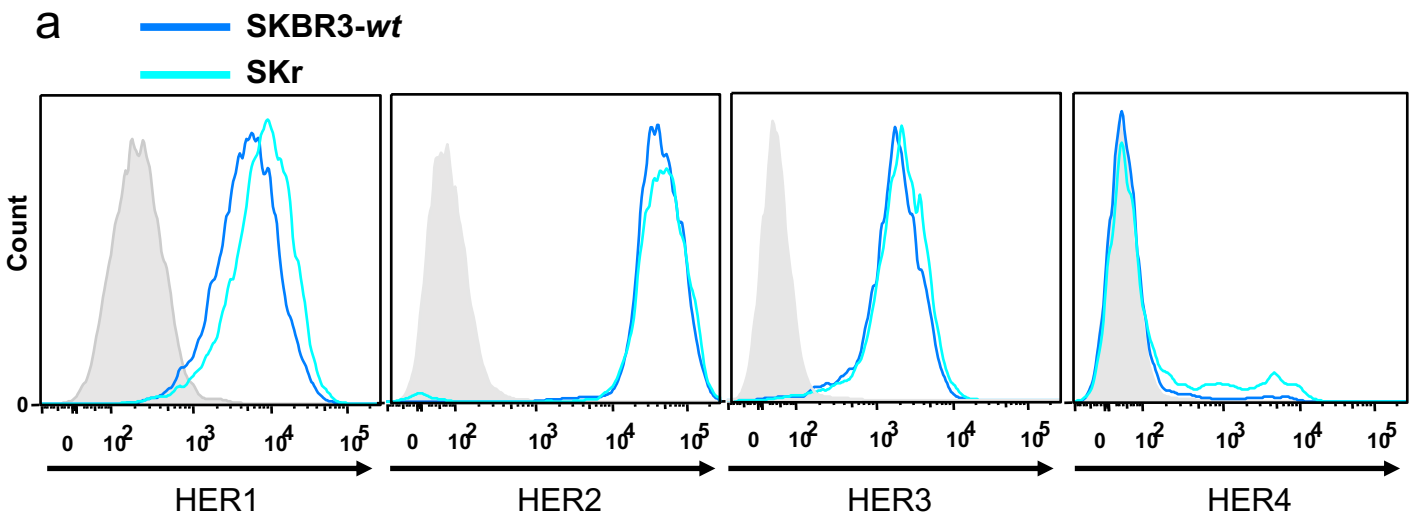

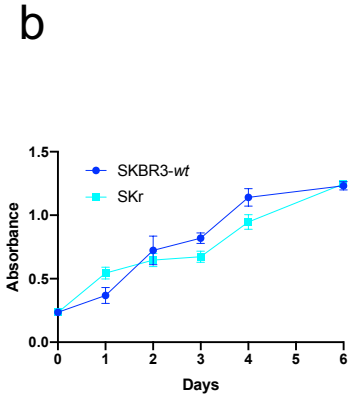

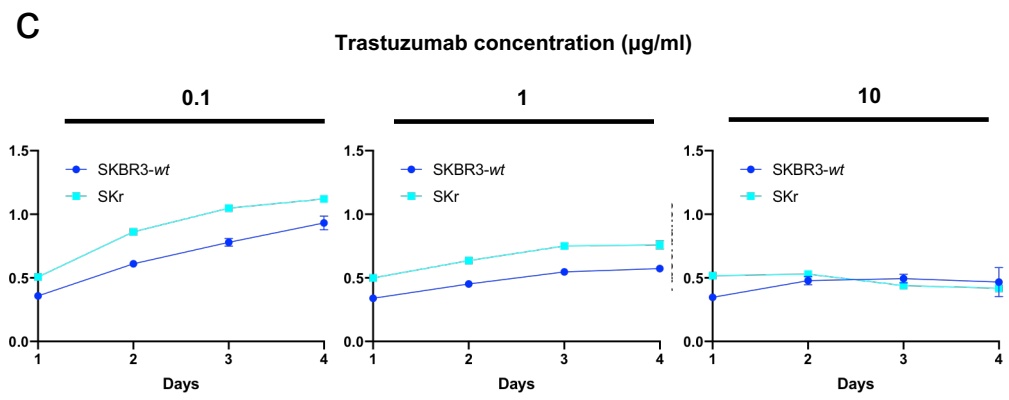

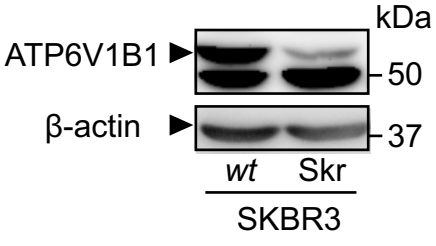

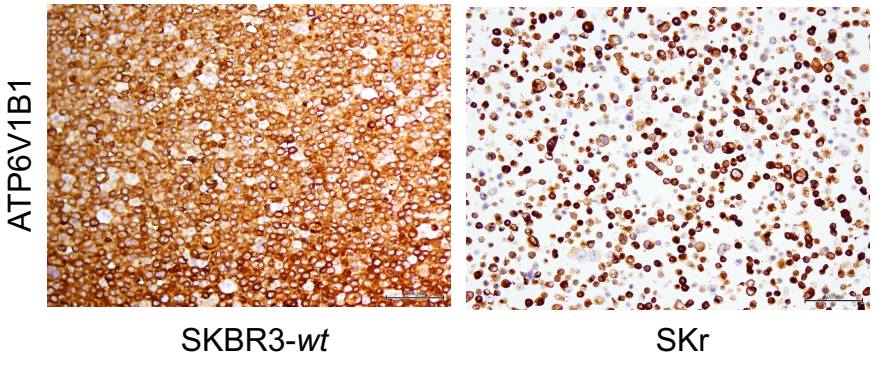

Supplementary Figure 2

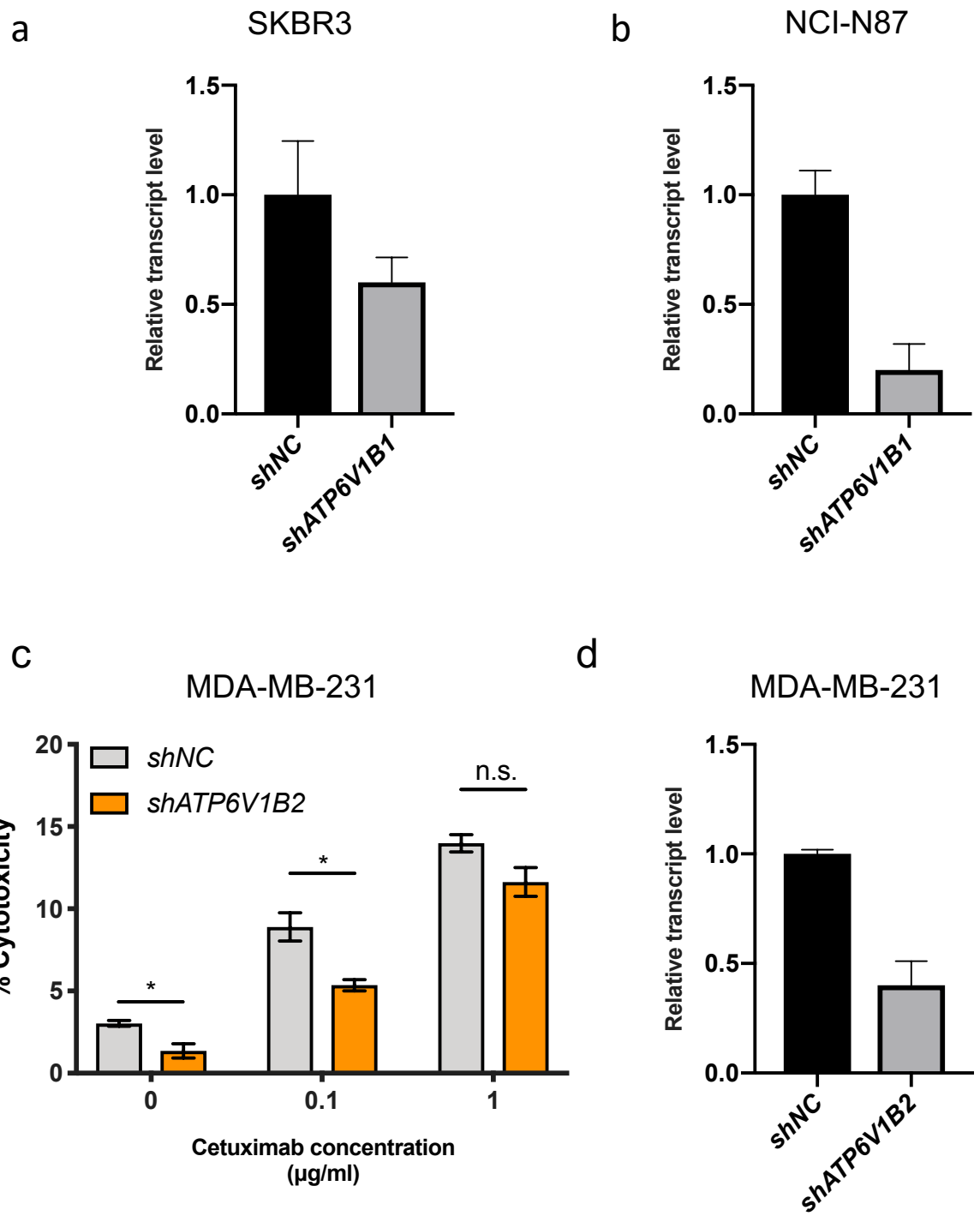

Supplementary Figure 3

a

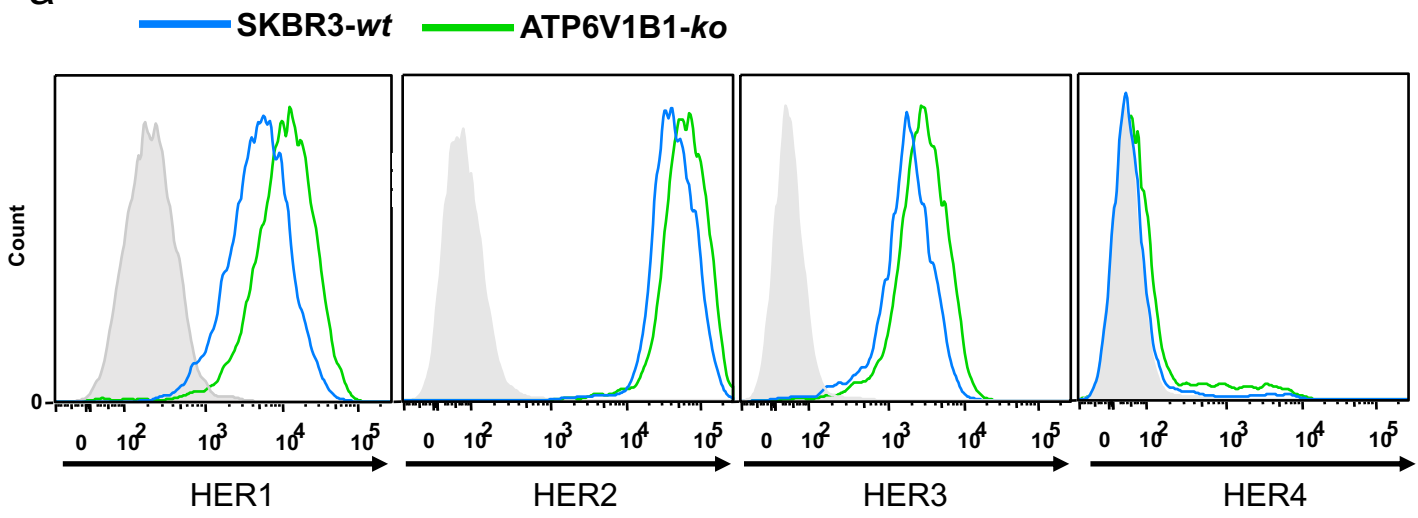

b

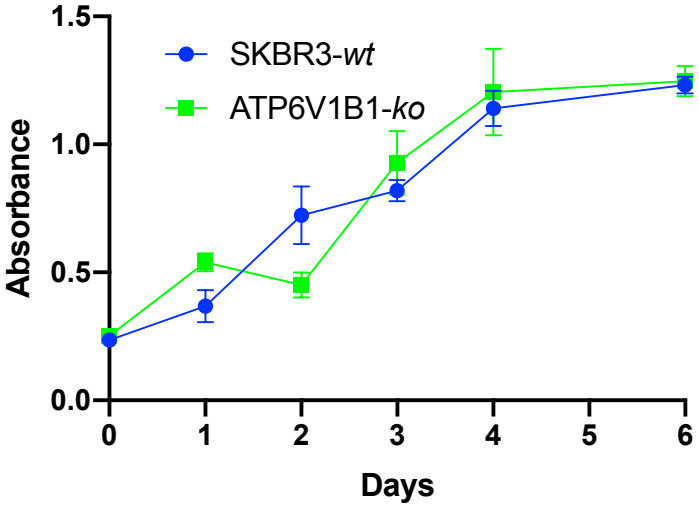

Supplementary Figure 4

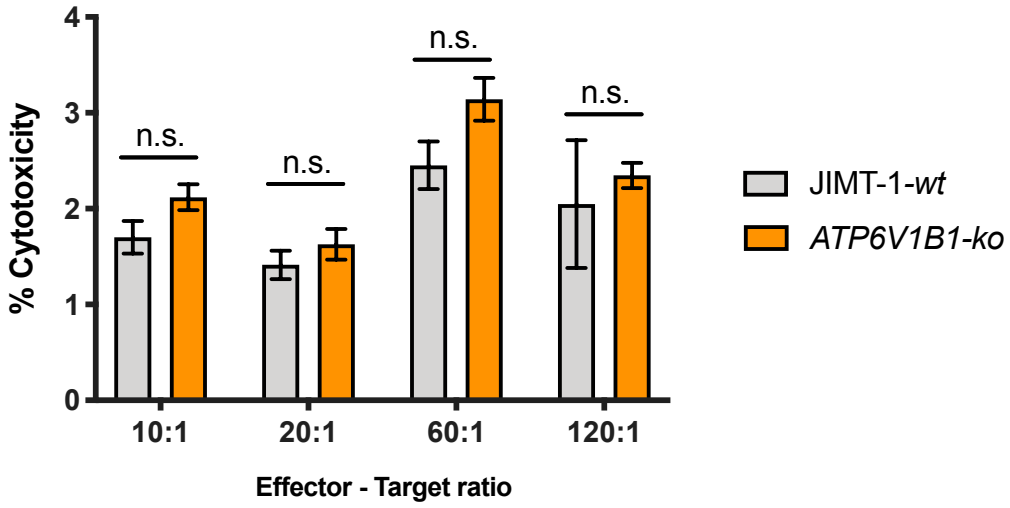

Supplementary Figure 5

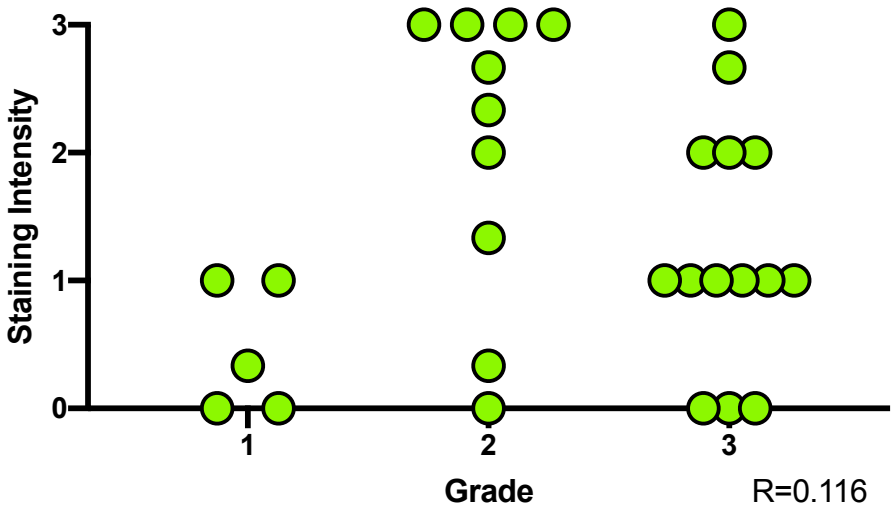

Figure legends

Supplementary Table 1. Comparison of gene expression levels between wild-type and ADCC-resistant SKBR3 cells according to RNA-sequencing data. All summarized gene counts other than those with raw counts over 10 reads per kilobase per million mapped reads were eliminated, and the intracellular pH-regulating genes with fold-changes of < 0.66 or >1.5 between wild-type and ADCC-resistant SKBR3 cells were selected. Raw RNA-sequencing data for the intracellular pH-regulating genes are presented.

Supplementary Figure 1.a) The abundance of HER family receptors (HER1, HER2, HER3, and HER4) of SKBR3 and SKr measured by flow cytometry. Grey is isotype control. **b)** Comparison of cell proliferation of SKBR3 and SKr analyzed by WST8 assay. **c)** Comparison of cell proliferation of SKBR3 and SKr under 0.1-10 μg/ml trastuzumab concentration by MTS assay. **d and e)** Protein abundance compared in a western blot (d) and by immunohistochemistry (e).

Supplementary Figure 2. a and b) Quantification of shRNA-mediated ATP6V1B1 knockdown in SKBR3 (a) and NCI-N87 (b) cells by qRT-PCR. **c)** Comparison of ADCC

in MDA-MB-231^{shATP6V1B2} and MDA-MB-231^{shNC} cells based on the LDH assay. The cytotoxicities of MDA-MB-231^{shATP6V1B2} and MDA-MB-231^{shNC} cells were 5.4% and 8.9%, respectively, in the presence of 0.1 μg/ml cetuximab ($p = 0.035$). **d)** Quantification of shRNA-mediated ATP6V1B2 knockdown in MDA-MB-231 cells. N = 3 for all experiments. *$p < 0.1$, ns:not significant. The graph shows mean ± SEM.

Supplementary Figure 3.a) The abundance of HER family receptors (HER1, HER2, HER3, and HER4) of SKBR3 and *ATP6V1B1*-KO cells measured by flow cytometry. Grey is isotype control. **b)** Comparison of cell proliferation of SKBR3 and *ATP6V1B1*-KO cells analyzed by WST8 assay. N = 3 for all experiments.

Supplementary Figure 4. The AICC activities of wild-type JIMT-1 cells and ATP6V1B1-KO cells were evaluated with an LDH assay after culturing at an effector-to-target ratio of 10: 1, 20: 1, 60:1 and 120: 1 for 4 hours. N = 3 for all experiments. ns: not significant. The graph shows mean ± SEM.

Supplementary Figure 5. Correlation between the staining intensity of ATP6V1B1 in

biopsy samples and the therapeutic effect of neoadjuvant chemotherapy (N=29).